frontiers | Frontiers in Earth Science

TYPE Original Research
PUBLISHED 29 February 2024
DOI 10.3389/feart.2024.1372537

OPEN ACCESS

EDITED BY
Pengjiao Jia,
Soochow University, China

REVIEWED BY
Jidong Teng,
Central South University, China
Zhen Wang,
Yangzhou University, China
Changshuo Wang,
Ningbo University, China
Ren Weizhong,
Chinese Academy of Sciences (CAS), China

*CORRESPONDENCE
Guangli Xu,
xu1963@cug.edu.cn

RECEIVED 18 January 2024
ACCEPTED 15 February 2024
PUBLISHED 29 February 2024

CITATION
Xue M, Xu G, Yao F and Ma Z (2024), Research on characteristics and geological genesis of large-scale deep-seated landslide in tuff formation.
Front. Earth Sci. 12:1372537.
doi: 10.3389/feart.2024.1372537

Research on characteristics and geological genesis of large-scale deep-seated landslide in tuff formation

Mengqi Xue[1], Guangli Xu[1,2]*, Feixiang Yao[3] and Zhuo Ma[4]

[1]Institute of Geological Survey, China University of Geosciences, Wuhan, China, [2]Faculty of Engineering, China University of Geosciences, Wuhan, China, [3]China United Engineering Corporation Limited, Hangzhou, China, [4]China Energy Engineering Group Yunnan Electric Power Design Institute, Kunming, China

In engineering practice, engineers generally treated tuff as a lumpy material with a poorly defined laminated structure and a rock group that was not susceptible to slide failure. Most studies of tuff landslides had focused on small clastic landslides in shallow strata with weathering boundaries and lithologic interfaces as slip surfaces. This paper takes a large-scale, deep-seated tuff landslide on the southeast coast of China as the research project. We used borehole TV imaging and exploration tunnels to confirm the material composition and structural characteristics of the tuff stratum and used exploration tunnels to expose the slip soil directly. Microscopic identification, mineralogical composition analysis, zircon U-Pb isotope dating, and Hf isotope analysis of slip soils collected from the exploration tunnels elucidated the geologic background and genesis of the large-scale deep-seated landslides in the tuff stratum. It was found that the formation of a tuff stratum in the landslide area was caused by multi-volcanic orogeny and multi-phase tectonics. The timing of the melting of the original magma from these volcanic events also differs. During these intervals between eruptions, deposition occurred, and this sedimentary material formed the slip soil.

KEYWORDS

large-scale landslide, deep-seated landslide, tuff, intermittent eruption, slip soil

1 Introduction

Volcanic activity is a potential geological force leading to global climate change and the extinction of biological populations (Rampino and Stothers, 1988; Olsen, 1999; Wignall, 2001). Tuff, one of the direct products of volcanic activity, is also a research hotspot at present (Benito et al., 1998; Xu et al., 2004; Hints R. et al., 2006; He et al., 2007). Tuff, which belongs to pyroclastic rock, is a transitional type between igneous rock and ordinary sedimentary rock and is thought to be formed after the fall of volcanic ash (Haaland et al., 2000; Grevenitz et al., 2003). The tuff stratum, in which landslides are generally developed, is widely distributed in the southeast coastal area of China. In Zhejiang Province, on the southeast coast of China, the Lidong landslide, Shanzao village landslide, and Xiabanling landslide caused more than 70 deaths, and the Xiageliao landslide caused potential economic losses of $62,640,000. The series of heavy and massive landslides and geological disasters have brought enormous damage and threats to people's lives, health, and property safety. Tuff normally, the igneous rock widely used as a natural building material, is considered hard rock without apparent stratum rationality. Therefore, tuff does not have the primary

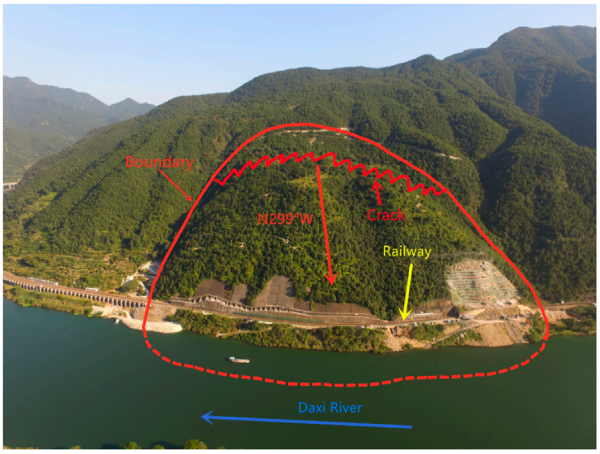

FIGURE 1
The basic situation of the Xiageliao landslide by aerial photograph.

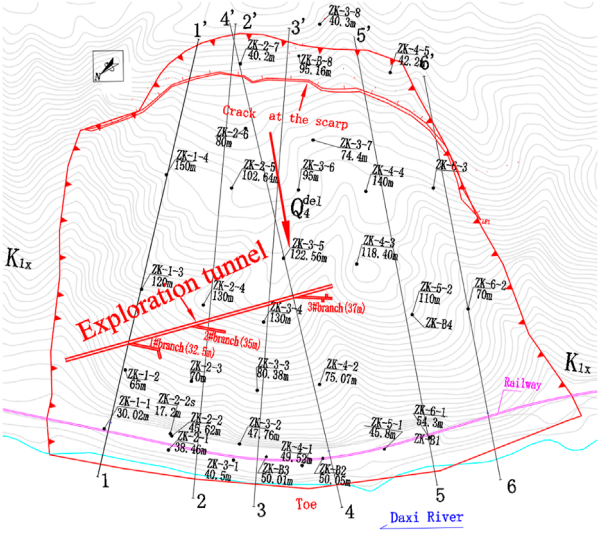

FIGURE 2
The plan for Xiageliao landslide.

conditions for many landslides. However, multiple tuff landslides above have occurred or are developing evidence that the tuff stratum is very suitable to breed large and even super large-scale deep-seated landslides.

There are few research studies on large-scale, deep-seated tuff landslides, which are still in the preliminary exploration stage. Used the X-ray diffraction method to determine the clay minerals composition of tuff from the Kunimi landslide and concluded that the content of clay minerals was higher in the groundwater enrichment zone of the landslide (Shuzui and Shimoda, 1987; Shuzui, 2001). When a landslide occurred in the tuff formation accompanied by continuous deformation, the content of clay minerals in the slip-surface continued to increase under the action of groundwater. In contrast, the content of detrital minerals decreased. It was the most critical factor in the decline of anti-sliding ability in slip-surface. Lu compared three landslides in the Cayley volcanic area in the United Kingdom and analyzed the similarities and differences between the tuff and dacite tuff landslides, including the slip-surface geotechnical properties and landslide motion forms (Lu, 1993). Trandafir et al. analyzed the formation mechanism of the Norwood Tuff landslide. They concluded that the landslide was a gradual destruction process due to the rise of groundwater level and human activities (Trandafir and Amini, 2009). Beisner et al. analyzed and studied the dynamic displacement characteristics of the Norwood Tuff landslide underwater level and seismic acceleration (Beisner, 2011). Hiroyuki et al. researched the Oshinkoshin landslide in Shiretoko Peninsula, eastern Hokkaido, Japan. They proposed that landslides were mainly controlled by the thick-hard shale with multiple thin strata of soft tuff (Maeda et al., 2014). Masahiro conducted a systematic study on the characteristics of deep-seated tuff landslides, considering the two influencing factors of rainfall and earthquakes (Masahiro, 2016).

We researched the Xiageliao landslide in Zhejiang Province, China. We used drilling, borehole photography, and tunnel exploration as the primary survey methods to study the large-scale, deep-seated tuff landslide characteristics. Some experiments were done to explain the relationship between landslides and tuff formation. Finally, a development model of the large-scale deep-seated tuff landslide was summarized.

2 Investigation and research on xiageliao landslide

As shown in Figure 1, Xiageliao landslide is located on the right bank of the Daxi River in Qingtian County, Zhejiang Province, on the southeast coast of China, with the foot of the slope submerging into the 38 m deep river water and a freight railway in the foot of the slope about 15 m above the river. The landslide was first discovered in 2012 when the retaining wall of the railway was cracked due to the deformation of the landslide, and the trains could only run at a speed of 26 km/h to ensure safety. In April 2016, a crack with a length of about 500 m and a width of about 0.5 m was discovered on the rear edge of the landslide, which caused the railway's suspension and residents' relocation.

Figure 2 and Figure 3 show that the main sliding direction of the landslide is about 299°, the length of the landslide is about 510 m, the width is about 580 m, the elevation is between 20 and 275 m above sea level, and the total area is about 200,000 m^2. The thickness of the landslide is 20–105 m, and the total volume of the landslide body is about 1100×10^4 m^3, so the landslide was defined as a large-scale, deep-seated landslide. To better study the Xiageliao landslide, we drilled 42 boreholes within the landslide area; these boreholes totaled 2976.17 m in length; the boreholes exposed the structural characteristics of the tuff and also provided good sampling conditions, see Figure 4A. Similarly, an exploration tunnel was constructed from the gully at the right boundary of the landslide, see Figure 4B. This tunnel consists of a 270 m-long main tunnel and three branch tunnels that cross the slip surface. The dimensions of the main tunnel were 3 m × 3 m, and the branch tunnels were 2.25 m × 2 m. The main tunnel provided more intuitive information about the structural changes of the slip body, and all three branch tunnels

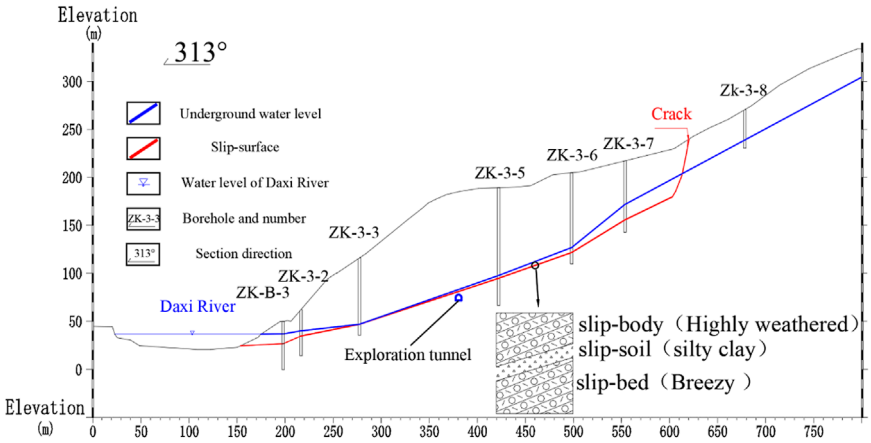

FIGURE 3
The profile of Xiageliao landslide (Section 3-3′).

FIGURE 4
Photographs of the core and exploration tunnel for the Xiageliao landslide. **(A)** Photographs of the core from the borehole. **(B)** Photographs of the exploration tunnel.

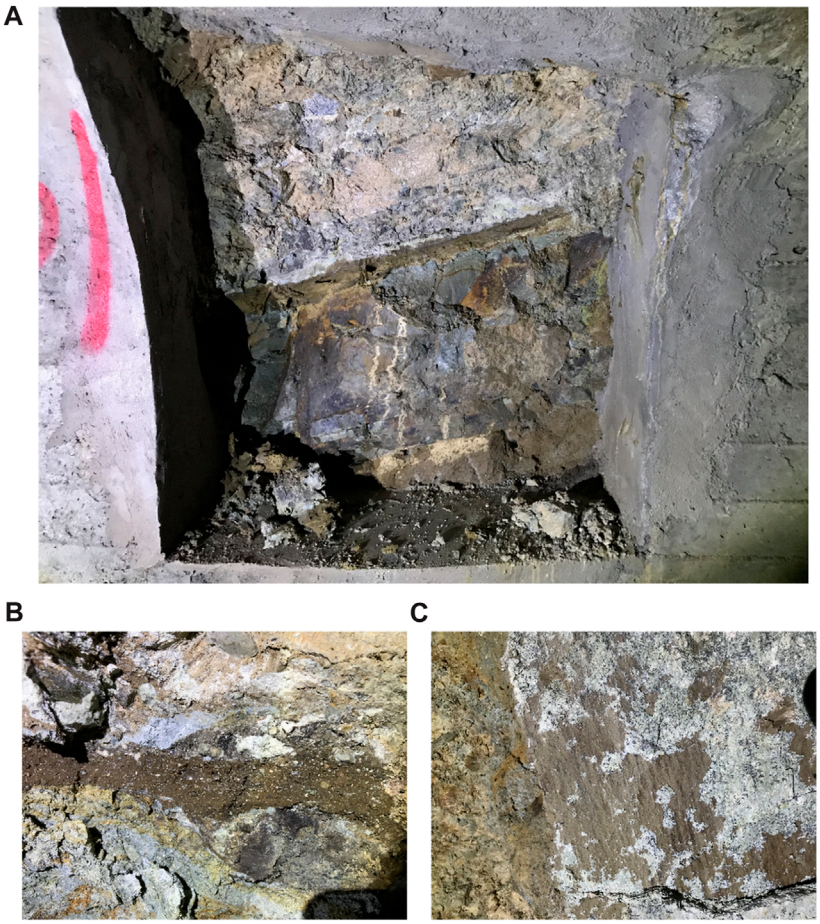

FIGURE 5
Slip soil revealed by exploration tunnels. **(A)** Distant view of slip soil. **(B)** Close-up of slip soil. **(C)** Scratch marks.

accurately revealed the location of the slip surface and provided good observation conditions and sampling conditions for the undisturbed slip soil.

Figure 5A presents the slip-surface observation window in 3# branch tunnel located about 100 m below the ground surface, and the slip-soil is a stratum of clay with a thickness of about 5–12 cm between the strongly weathered slip-body and the slightly weathered slip-bed. Figure 5B shows a close-up of slip-soil with occurrence 295°∠21°which, which is yellow-brown clay with a thickness of 3–15 cm. The slip-soil is relatively dense with a slippery feel, hard plastic-soft plastic, and easy to soften in contact with water, leading to the local seepage area. Figure 5C shows a close-up of slip-soil scratches. The width of the groove is about 2 mm, and the scratch direction is 300°, which is consistent with the sliding direction of the landslide, so this clay stratum is the slip-soil.

The Xiageliao landslide is developed in the Cretaceous (K_1x) tuff stratum. In this paper, the exploration results of borehole zk3-5, located in the middle of the landslide, were selected to be presented and studied. Figure 5 presents the basic situation of the landslide tuff formation. Figure 6A is a schematic diagram for the stratum structure of borehole ZK3-5 and shows that the tuff formation above the slip-bed has alternated between broken and intact many times. This situation was also found in other boreholes, and according to data collection, this phenomenon also occurred in areas outside the landslide range. Figure 6B shows the partial results by borehole TV imaging in borehole ZK3-5, and in the 64–76 m section of ZK3-5, the complete fragmentation (strong-medium weathered) of the tuff changes many times. While macroscopic observations of the stratigraphic structure of the tuff stratum were made through boreholes, core samples were also sampled and numbered according to s1 to s8. The specific sampling location can be seen in the dotted line position in Figure 6A.

To explore the performance of the landslide tuff on the micro level, eight sets of core samples from the borehole ZK3-5 were selected for microscopic identification. The sampling locations are shown in Figure 6A. The microscopic identification instrument was a microscope (OLYMPUS BX51, China University of Geosciences (Wuhan)); the results are shown in Figure 7. S-1 sampling depth of 8.5 m was identified as light metamorphic dacite lithic-crystal tuff, mainly composed of crystal fragments, detritus, and volcanic ash. The crystal fragment was locally altered by weathering and is mainly composed of quartz and feldspar. S-2 sampling depth of 24.4 m was identified as light metamorphic dacite lithic-crystal tuff, similar to s-1. The plagioclase in the sample was weathered and altered under the action of late stress. The late extensional fissure interspersed the fractional crystal fragment, and along both sides of

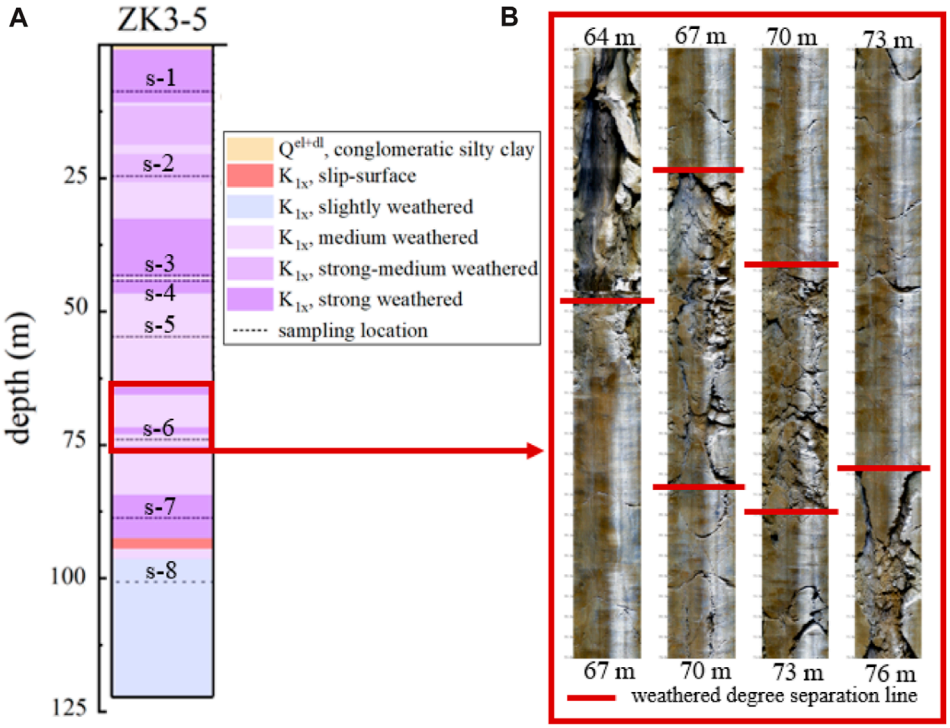

FIGURE 6
Stratum structure characteristics of Xiageliao landslide. **(A)** Schematic diagram of the core structure of the borehole. **(B)** Borehole TV images.

the fissure, the weathering and erosion became intense. Part of the feldspars were eroded into sericite and clay minerals. The detritus are mainly quartzite debris in mid-late rock. S-3 sampling depth 43 m was identified as lithic crystal tuff, mainly composed of crystal fragments, detritus, and volcanic ash; the rock crystal fragment was strongly weathered and altered. Quartz veins were squeezed to relax, wave-like are developed in the rock, and partial quartz veins were compressed to form a stone sausage structure. It shown a soft-hard inter-stratum structure in this area. S-4, with a sampling depth of 43.8 m, was identified as lithic crystal tuff, similar to s-3, and the crystal fragment was mainly feldspar and quartz. Quartz veins with compression and torsion characteristic are developed. Figure S-5, sampling depth 54.5 m, identified as rhyolitic lithic-crystal tuff with malleable rhyolite structure mainly composed of crystal fragments, detritus, and volcanic ash. Quartz sericite had an obvious intermittent orientation. S-6 sampling depth of 73.8 m was identified as silicified crystal lithic tuff. The robust, weathered rock presented a silicified state with small, interspersed, compressed quartz veins. Figure S-7 sampling depth 88.5 m was strong weathered tuff in slip-surface, and the basic was lithic crystal tuff. The crystal fragment is mainly quartz (15%), followed by feldspar (7%), and sericite is well-developed. S-8 sampling depth 99.5 m was medium weathered tuff in slip-bed identified as lithic crystal tuff with mainly larger particle size plagioclase crystal fragment with a reasonable degree of self-shape with glassy tuff vein partially interspersed.

The tuff in the landslide area is mainly composed of lithic crystal tuff, of which the shallow part is composed chiefly of dacite tuff, and the deep stratum is mostly basic rhyolitic tuff. The degree of weathering is quite different at different depths, and the crystal fragments and veins also show that some stratum from different depths are subject to more significant compression stress. It indicates that the later geological forces suffered by tuff strata are of different periods. Similarly, the different types of tuff in each stratum also reveal that the volcanic structures that formed these tuff stratum were different.

With the identification of the Xiageliao landslide's characteristics, the research's core issue is: Why did the volcanic tuff formation without apparent stratification give birth to large-scale deep-seated landslides like the Xiageliao landslide? This problem can be divided into two aspects. The first is to determine how such a complex tuff formation is formed, and the second is to determine the formation of a continuous clay slip surface about 100 m below the surface. For this purpose, three experiments were designed in this study: age dating, isotope analysis, and compositional determination of tuff.

3 Materials and methods

3.1 *In-situ* U-pb dating of zircon by LA-ICP-MS

Zircon is a relatively common by-mineral, commonly found in magmatic rocks, with a stable crystal structure and high stability of closure, which has the property of persistently maintaining the physical and chemical characteristics of the mineral at the time of its

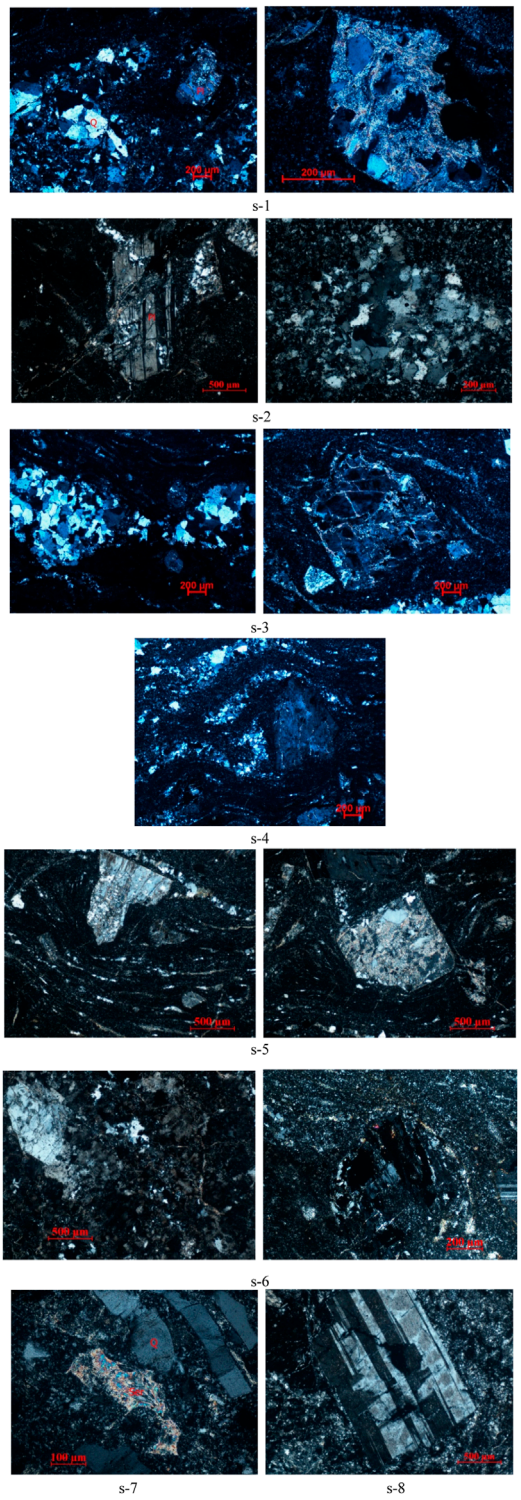

FIGURE 7
Micrographs of tuff at different depths of the Xiageliao landslide.

formation and its structure and composition reflect the geological processes experienced by the rock. The high U and Th content of zircon makes it the most frequently studied object in U-Pb isotope geochronology, and zircon dating utilizes the decay of U and Th isotopes into Pb isotopes. To analyze the evolutionary history and characteristics of the geotechnical bodies in the landslide area, more than 20 sets of rock samples were taken from 6 boreholes at different depths in the 3–3′ section of the landslide and from the rock layers above and below the landslide zone and analyzed for zircon U-Pb dating. The zircon U-Pb isotope dating and trace element content were analyzed using the LA-ICP-MS method, which is commonly used nowadays.

Zircon U-Pb isotopic dating, Hf isotope determination, and X-ray diffraction analysis were designed to explain the complex stratification of the tuff in the landslide area and to validate the hypothesis about the formation of the tuff. The samples were taken from the cores in boreholes of different depths, and the undisturbed slip-soil samples were taken directly from the exploration tunnel.

Figure 8 shows the photos of zircon U-Pb dating samples and selected points of zircon CL images of zircon tuffs in the landslide area; the red circles in the picture show laser test chosen points. Zircons were selected from core samples from different locations in different boreholes. Then, the tuff samples were crushed, and single-grained zircons were randomly chosen by gravity and magnetic sorting to avoid artificial selectivity as much as possible. These zircons were then spaced so that they were independent of each other, arranged in an orderly manner, and finally made into targets. Transmitted light, reflected light, and cathodoluminescence (CL) images were taken of the zircon targets, and zircons with good crystal shape and transparency were selected as the basis for the zircon dating analysis. Finally, the pointing and data processing were carried out.

U-Pb dating of zircon was conducted by LA-ICP-MS. Laser sampling was performed using a GeolasPro laser ablation system that consists of a COMPexPro 102 ArF excimer laser (wavelength of 193 nm and maximum energy of 200 MJ) and a MicroLas optical system. An Agilent 7700e ICP-MS instrument was used to acquire ion-signal intensities. The spot size and frequency of the laser were set to 32 μm and 5 Hz, respectively, in this study. Detailed operating conditions for the laser ablation system and the ICP-MS instrument and data reduction are the same as description by (Liu et al., 2008; Liu et al., 2010; Hu et al., 2015; Zong et al., 2017). Zircon 91,500 and glass NIST610 were used as external standards for U-Pb dating and trace element calibration, respectively. Each analysis incorporated a background acquisition of approximately 20–30 s, followed by 50 s data acquisition from the sample. An Excel-based software, ICPMSDataCal, was used to perform off-line selection and integration of background and analyzed signals, time-drift correction, and quantitative calibration for trace element analysis and U-Pb dating (Liu et al., 2008; Liu et al., 2010)17,18. Concordia diagrams and weighted mean calculations were made using Isoplot/Ex_ver3 (Ludwig, 2003).

3.2 Hf isotope ratio analyses by LA-ICP-MS

The zircon samples used in this experiment were also derived from the age-determined zircon in the previous section. These zircons were pre-treated and analyzed for Hf isotopes. All chemical preparations were performed on class 100 work benches within a class 1000 over-pressured clean laboratory. Sample digestion: (1) Sample powder (200 mesh) was placed in an oven at 105°C

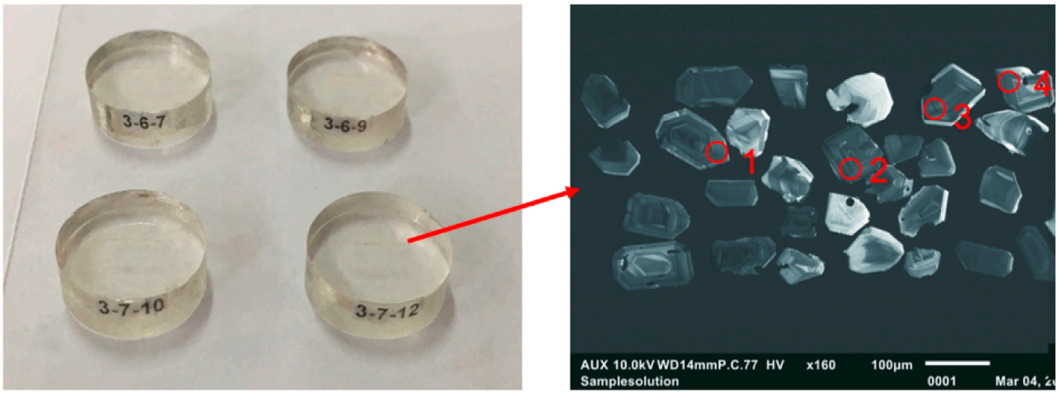

FIGURE 8
Zircon target and CL camera view.

for drying of 12 h; (2) 50–200 mg sample powder was accurately weighed and placed in a Teflon bomb; (3) 1–3 mL HNO_3 and 1–3 mL HF were added into the Teflon bomb; (4) Teflon bomb was put in a stainless steel pressure jacket and heated to 190°C in an oven for >24 h; (5) After cooling, the Teflon bomb was opened and placed on a hotplate at 140°C and evaporated to incipient dryness, and then 1 mL HNO_3 was added and evaporated to dryness again; (6) The sample was dissolved in 3.0 M HF. Column chemistry: After centrifugation, the supernatant solution was loaded into an ion exchange column packed with LN-Spec resin. After complete draining of the sample solution, columns were rinsed with 3 M HCl, 6 M HCl, and 4 M HCl+H_2O_2 (0.5%) to remove undesirable matrix elements. Finally, the Hf fraction was eluted using 2.0 M HF and gently evaporated to dryness before mass-spectrometric measurement.

Experiments of *in situ* Hf isotope ratio analysis were conducted using a Neptune Plus MC-ICP-MS (Thermo et al.) in combination with a Geolas HD excimer ArF laser ablation system (Coherent, Göttingen, Germany). The laser energy is 8 mJ/cm^2, the frequency is 8 Hz, and the laser beam spot diameter is 44 μm. Detailed instrument operating conditions and analysis methods can be referred to (Hu et al., 2012). This laser ablation system includes a "wire" signal smoothing device, producing smooth signals even at meager laser repetition rates down to 1 Hz. Helium was used as the carrier gas within the ablation cell and was merged with argon (makeup gas) after the ablation cell. Small amounts of nitrogen were added to the argon makeup gas flow to improve the sensitivity of Hf isotopes (Hu et al., 2012). Off-line selection, analysis of analyte signals, and mass bias calibrations were performed using ICPMSDataCal (Liu et al., 2010).

3.3 X-ray diffraction test

The XRD test was commissioned by the State Key Laboratory of Geological Processes and Mineral Resources (China University of Geosciences), and the instrument model is X'Pert PRO DY2198. The test samples were slip soils and tuffs above and below them, taken from the exploration tunnels.

Samples for XRD analysis were crushed coarsely and moderately; after grinding, the samples were ground to 200 mesh with a mortar and pestle. After grinding, the samples were dried at 105 °C, and 5 g were weighed accurately. After drying at 105°C, 5 g of the sample was weighed accurately and placed in a crucible. After the sample was dried at 105°C, 5 g was weighed accurately and placed in a crucible. A mixture of lithium tetraborate-lithium metaborate-lithium nitrate was added to the crucible. After confirming that the sample and the melt were thoroughly mixed, the sample was melted in a high-precision melting furnace at 1050°C. The molten slurry was poured into a platinum model, cooled to form a fused sheet, and then analyzed by X-ray diffraction.

Then X-ray diffraction analysis was performed. The experimental conditions were as follows: voltage 40kV, current 40 mA, 2θ angle from 5° to 60°, step size of 0.04°/step, and scanning speed of 5 s/step. The scanning speed was 5 s/step. The accuracy of the goniometer was less than 0.01° (2θ angle), and the detection limit of mineral content was about 1%. The accuracy of the goniometer is less than 0.01° (2θ angle), and the detection limit of the mineral content is about 1%. Mineral species were analyzed using JADE6.5 software with standard curves of various minerals. The mineral species were determined by comparing them with the standard curves of various minerals using JADE6.5 software. In the XRD test, high-purity silica powder was chosen as the calibration standard, and the 2θ angle of the sample to be tested was calibrated by the external standard method. In the XRD test, high-purity silica powder was chosen as the calibration standard, and the 2θ angle of the sample to be tested was corrected by the external standard method. The standard sample and the sample to be tested were analyzed with the same instrument and under the same experimental conditions. The standard sample and the sample to be tested were diffracted with the same instrument and under the same experimental conditions, and the data of the standard sample were compared with the standard values. The data of the standard sample was compared with the standard value to find out the correction value of each 2θ angle. Then the 2θ angle of the measured sample was corrected by the external traditional method. Then, the 2θ angle of the measured sample is fixed.

TABLE 1 Laboratory test results on samples from the Xiageliao landslide.

Sample number	Sample position	Depth of slip-surface(m)	Sample identification	U-Pb isotopic data of zircons from tuff				Hf isotopic data of zircons from tuff	
				Concordia age (Ma)	MSWD	Weighted mean age (Ma)	Concordance (%)	T_{dm1} (Ma)	T_{dm2} (Ma)
3-6–5	borehole ZK3-6 (50.8 m)	78.9	Rhyolitic Crystal Tuff	124.55 ±0.85	4.63	124.5 ± 1.1	95	1124.81–1293.73	1854.72–1947.32
3-6–7	borehole ZK3-6 (61.4 m)		Lithic Crystal Tuff	127.86 ±0.32	2.7	127.85 ± 0.85	95	1202.87–1463.35	1837.98–2164.73
3-6–9	borehole ZK3-6 (89.8 m)		Tuff	128.9 ± 1.0	0.99	130.5 ± 1.3	95	1191.05–1495.59	1805.75–2259.83
3-7–3	borehole ZK3-7 (10.9 m)	59.7	Dacitic Tuff	128.28 ±1.1	2.2	128.3 ± 1.5	95	1241.90–1338.94	1906.68–2025.25
3-7–4	borehole ZK3-7 (18.8 m)		Biotite Dacitic Crystal Fragment Tuff	130.8 ±0.50	1.11	130.76 ± 0.98	95	1223.50–1285.44	1866.24–1925.32
3-7–10	borehole ZK3-7 (49.6 m)		Rhyolitic Crystal Tuff	130.33 ±1.1	7.2	130.3 ± 1.4	95	1276.05–1511.88	1946.68–2193.58
3-7–12	borehole ZK3-7 (64.5 m)		Lithic Crystal Tuff	132.52 ±0.40	1.4	132.52 ± 0.97	95	1179.22–1467.35	1798.98–2200.27

10.3389/feart.2024.1372537

TABLE 2 U-Pb isotopic data of zircons from the Xiageliao landslide.

Sample number	Th232 ppm	U238 ppm	207Pb/206 Pb	207 Pb/235U	206 Pb/238U	208Pb/232Th	238U/232Th
			Ratio	Ratio	Ratio	Ratio	Ratio
3-6–5	450.52 ± 149.14	484.63 ± 171.78	0.05 ± 0.013	0.13 ± 0.004	0.02 ± 0.001	0.006 ± 0.001	0.19 ± 0.134
3-6–7	560.54 ± 495.140	337.80 ± 256.632	0.05 ± 0.002	0.13 ± 0.007	0.02 ± 0.001	0.006 ± 0.001	0.79 ± 0.229
3-6–9	308.32 ± 145.76	308.55 ± 171.82	0.07 ± 0.017	0.19 ± 0.060	0.02 ± 0.001	0.006 ± 0.001	1.07 ± 0.511
3-7–3	584.76 ± 470.915	358.95 ± 234.855	0.05 ± 0.003	0.14 ± 0.008	0.02 ± 0.001	0.006 ± 0.001	0.88 ± 0.446
3-7–4	578.90 ± 427.72	477.84 ± 427.721	0.05 ± 0.003	0.14 ± 0.008	0.02 ± 0.001	0.006 ± 0.001	0.87 ± 0.429
3-7–10	634.57 ± 289.973	467.84 ± 156.502	0.05 ± 0.003	0.14 ± 0.009	0.02 ± 0.001	0.006 ± 0.001	0.91 ± 0.376
3-7–12	291.63 ± 213.878	317.59 ± 221.683	0.05 ± 0.003	0.14 ± 0.009	0.2 ± 0.001	0.007 ± 0.001	1.02 ± 0.373

4 Results

According to Table 2, the Th/U values of zircons in the Xiageliao landslide range from 0.58 to 2.19, with an average value of 1.28, which is significantly greater than 0.1, indicating an apparent magmatic origin (Koschek, 1993). Tables 1 and 2 show the U-Pb zircon date results of the tuff at different depths. The Xiageliao landslide's tuff belongs to the lower Cretaceous stratum, and the test results show that the adjacent tuff stratum (15–20 m interval) has an age difference of about 1–2 Ma. This proves the multi-period eruption theory of the landslide formation mentioned above. The volcanic activity that formed the landslide tuff stratum was frequent with short intervals. According to the top and bottom stratum of the slip surface (e.g., samples 3-7-3 and 3-7–5), the age difference between the two strata is about 1 Ma, more significant than that of the tuff stratum under the same conditions in the slip-body. It is evidenced that the intervals of volcanic activity after the tuff formation as slip-bed was more prolonged than other periods. Because of the long quiet period (3.5 Ma), this tuff area received sedimentation and weathering to form the original slip-soil material.

Table 1 and Table 3 show that the 176Lu/177Hf value of zircon from the landslide tuff is 0.000669–0.003317, which is smaller than the 176Lu/177Hf (0.0093) value of the upper crust (Vervoort et al., 1996). The 176Hf/177Hf value is 0.282210–0.282417. The average value is 0.282333, and fLu/Hf = −0.98~-0.90, which is less than the value of mafic crust value (−0.34) and silica-aluminum crust value (−0.72) (Vervoort et al., 1996; Amelin et al., 2000). The εHf(t) ranges from −17.13 to −9.71, indicating that the zircon originated from the re-melting of the ancient crust. The samples' two-stage model age (T_{dm2}) can better reflect when tuff was extracted from the depleted mantle or the mean age of source rock in the crust. The two-stage model age is between 1798.98 Ma and 2193.58 Ma, which belongs to the Paleoproterozoic and extends from the early Paleoproterozoic to the middle and late Paleoproterozoic. Although the εHf(t) of each sample is negative, the variation interval of the εHf(t) is eight ε units, which exceeds the error caused by the analysis method (Wu et al., 2006). The magma heterogeneity should cause it (Bolhar et al., 2008; Mo et al., 2009). Combined with the calculation results of the two-stage model age, it can be concluded that the magma formed tuff is from the continental crust material, but the specific material source, melting time, and volcanic edifice are different.

For the analysis of the mineralogical composition of the landslide material, we took two samples of tuff from the slip body above the slip soil, one sample of yellowish-brown slip soil, one sample of greenish-gray tuff that had been clayed under the slip soil, and two samples of tuff from the slip bed from the exploration tunnels. The test results of these samples can be seen in Figure 9, numbered A to F in that order.

Figures 9A,B presents slip-body tuff, and Figures 9E,F shows slip-bed tuff. The tuff has low clay mineral content (14.2%–30.8%) and very high clastic mineral content, especially quartz (50.8%–58.6%), typical volcanic clastic rock. Figures 9C,D shows the result as clay, among which Figure 9C is slip-soil with the highest clay mineral content (41.2%) and the lowest quartz content (16.01%). Although Figure 9D shows the result as clay-like, the overall mineral composition, especially the quartz content, differs significantly from the surrounding tuff and has prominent inheritance characteristics. It can be judged as the weathering

TABLE 3 Hf isotopic data of zircons from the Xiageliao landslide.

Sample number	Hf176/Hf177	Lu176/Hf177	εHf(t)	fLu/Hf
3-6–5	0.28238 ± 0.00002	0.00138 ± 0.00059	−11.38512 ± 0.78866	−0.95558 ± 0.00442
3-6–7	0.28233 ± 0.00007	0.00177 ± 0.00110	−12.98760 ± 2.60296	−0.94675 ± 0.03309
3-6–9	0.28231 ± 0.0010	0.00134 ± 0.00043	−13.45365 ± 3.68028	−0.95914 ± 0.01283
3-7–3	0.28235 ± 0.0003	0.00120 ± 0.00040	−12.40956 ± 0.94716	−0.96382 ± 0.01200
3-7–4	0.28238 ± 0.00001	0.00165 ± 0.00053	−11.25333 ± 0.46768	−0.95029 ± 0.01604
3-7–10	0.28230 ± 0.00005	0.00215 ± 0.00117	−14.05297 ± 1.96205	−0.93517 ± 0.03509
3-7–12	0.28233 ± 0.0009	0.00140 ± 0.00058	−12.89645 ± 3.18181	−0.95770 ± 0.01742

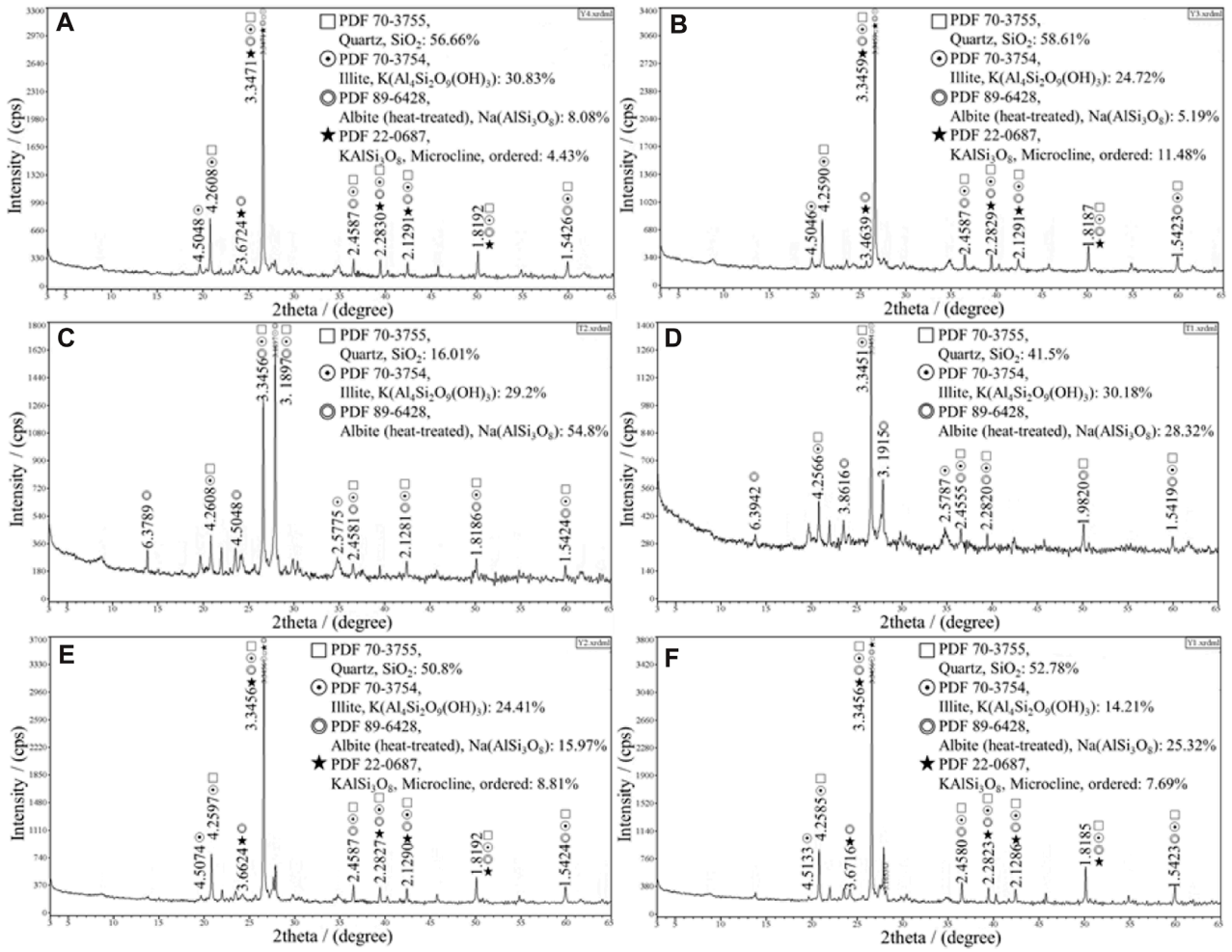

FIGURE 9
Mineral composition analysis of landslide material. **(A)** Tuff of the slip- body. **(B)** Tuff above slip soil. **(C)** Yellow-brown slip soil. **(D)** Greenish gray clay below slip soil. **(E)** Slip-bed tuff. **(F)** Slip-bed tuff.

disintegration production of tuff. After field identification and laboratory observation, no significant diagenetic signs and no rock skeleton were found in the slip-soil (Figure 9C). The content of quartz (Figure 9C) is much lower than that of tuff or its hydrolyzed clay (Figure 9 (d)). As a very stable mineral, quartz is unlikely to disappear due to weathering and hydrolysis. Similarly, quartz cannot be migrated out in such an occurrence environment. In other words, this yellow-brown clay did not develop from tuff, and these two are not homologous. It is not possible that the tuff formation was followed by the formation of a continuous

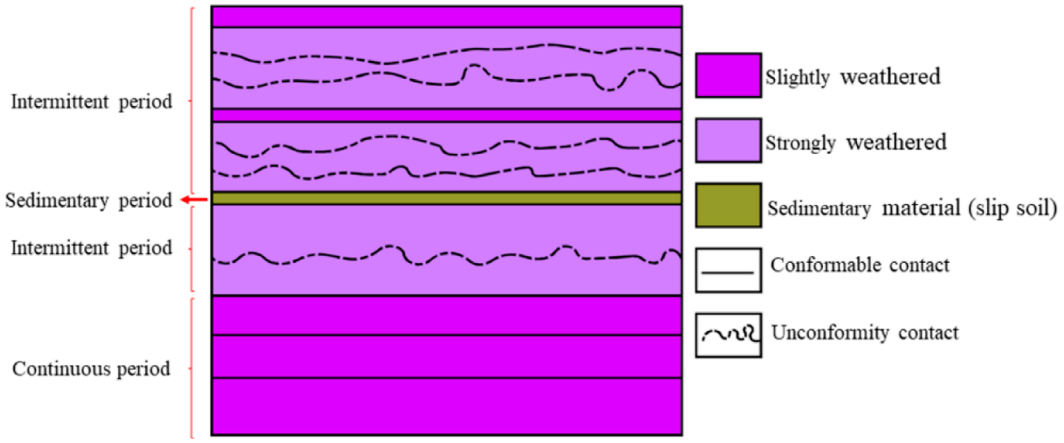

FIGURE 10
Model diagrams of tuff and slip soil formation.

clay stratum 90 m deep from the external material. It can only be formed in the early Cretaceous with tuff, and it is inferred that it is the production of sedimentary material during the eruption interval.

5 Conclusion

After the investigation and test results of the Xiageliao landslide, the following conclusions are drawn:

(1) The Xiageliao landslide was developed in a complex set of tuff strata. The tuff in the landslide area consisted of many different types with different levels of weathering. Through microscopic identification, it is found that these tuffs at different depths have different tectonic traces. This indicates that the formation of the tuff strata in the landslide area results from multiple volcanic activities and phases of tectonic action.

(2) The slip surface of the Xiageliao landslide is a continuous layer of yellowish-brown clay with a maximum depth of 90 m. By comparing the mineral composition of the slip soil and the tuff above and below it, it can be seen that it is not a product of tuff disintegration and weathering but was formed by the deposition of external materials. Combined with the location of the slip soils and the zircon dating results, the slip soils should be the products of sediments deposited during the intervals of volcanic activities.

(3) According to zircon dating, the tuffs at different depths are close in age of formation, but there is still a particular age gap. Combined with the microscopic identification and other auxiliary results, it can be concluded that several volcanic activities with short intervals formed this group of stratum. These volcanic activities were partially subjected to sedimentation during quiet periods. Similarly, during the quiet periods, the tuff strata that had been formed at that time were subjected to weathering and tectonic activities, resulting in the recurrence of strongly weathered and weakly weathered tuffs.

(4) According to Hf isotope analysis, more than one volcanic activity formed the tuff, and the melting time of the original magmatic material from these volcanic activities varied at different times. This explains the complex variations in tuff types and compositions in the landslide area.

Based on the above conclusions about the Xiageliao landslide, we can summarize the mechanism by which the tuff formed a large-scale deep-seated landslide, as shown in Figure 10. The multiple volcanic activities that formed the tuff stratum occurred discontinuously, with partially longer quiet periods long enough to receive enough sedimentary material. The repeated occurrence of this continuous eruption-interrupted process creates a complex stratum assemblage. When external conditions such as tectonic movements, river incision, and artificial slope cutting are appropriate, landslides can occur along the weak interlayers of sedimentary or weathered strata formed during the eruption-pause process as rainfall or groundwater changes.

Data availability statement

The original contributions presented in the study are included in the article/Supplementary Material, further inquiries can be directed to the corresponding author.

Author contributions

MX: Conceptualization, Data curation, Formal Analysis, Funding acquisition, Investigation, Methodology, Project administration, Resources, Software, Supervision, Validation, Visualization, Writing–original draft, Writing–review and editing. GX: Data curation, Investigation, Methodology, Project administration, Writing–review and editing. FY: Investigation, Data curation, Methodology, Writing–review and editing. ZM: Data curation, Investigation, Writing–review and editing.

Funding

The author(s) declare financial support was received for the research, authorship, and/or publication of this article. This study was supported by the project "Research on Characteristics and Prevention Technology of Large-scale Deep-seated Tuff Landslide (2017K03)" from China Railway Siyuan Survey and Design Institute Group Corporation Limited. We are very grateful for this.

Conflict of interest

Author FY was employed by China United Engineering Corporation Limited. Author ZM was employed by China Energy Engineering Group Yunnan Electric Power Design Institute.

The remaining authors declare that the research was conducted in the absence of any commercial or financial relationships that could be construed as a potential conflict of interest.

Publisher's note

All claims expressed in this article are solely those of the authors and do not necessarily represent those of their affiliated organizations, or those of the publisher, the editors and the reviewers. Any product that may be evaluated in this article, or claim that may be made by its manufacturer, is not guaranteed or endorsed by the publisher.

References

Amelin, Y., Lee, D. C., and Halliday, A. N. (2000). Early-middle Archaean crustal evolution deduced from Lu-Hf and U-Pb isotopic studies of single zircon grains. *Geochim. Cosmochim. Acta* 64, 4205–4225. doi:10.1016/S0016-7037(00)00493-2

Beisner, K. E. (2011). "Dynamic displacement analysis of a shallow landslide in Norwood tuff," in *First international symposium on uncertainty modeling and analysis and management (ICVRAM 2011) and fifth international symposium on uncertainty modeling and anaylsis (ISUMA)* (The University of Utah ProQuest Dissertations Publishing). Available at: https://ascelibrary.org/doi/epdf/10.1061/41170%28400%2980.

Benito, R., Garcia-Guinea, J., Walle-Fuentes, F. J., and Recio, P. (1998). Mineralogy, geochemistry and uses of the mordenite–bentonite ash-tuff beds of Los Escullos, Almeria, Spain. *J. Geochem. Explor.* 62, 229–240. doi:10.1016/S0375-6742(97)00075-7

Bolhar, R., Weaver, S. D., Whitehouse, M. J., Palin, J. M., Woodhead, J. D., and Cole, J. W. (2008). Sources and evolution of arc magmas inferred from coupled O and Hf isotope systematics of plutonic zircons from the Cretaceous Separation Point Suite (New Zealand). *Earth Planet. Sci. Lett.* 268, 312–324. doi:10.1016/j.epsl.2008.01.022

Grevenitz, P., Carr, P., and Hutton, A. (2003). Origin, alteration and geochemical correlation of late permian airfall tuffs in coal measures, Sydney basin, Australia. *Int. J. Coal Geol.* 55, 27–46. doi:10.1016/S0166-5162(03)00064-8

Haaland, H. J., Furnes, H., and Martinsen, O. J. (2000). Paleogene tuffaceous intervals, Grane field (block 25/11), Norwegian north sea: their depositional, petrographical, geochemical character and regional implications. *Mar. Pet. Geol.* 17, 101–118. doi:10.1016/S0264-8172(99)00009-4

He, B., Xu, Y., Huang, X., Luo, Z., Shi, Y., Yang, Q., et al. (2007). Age and duration of the Emeishan flood volcanism, SW China: geochemistry and SHRIMP zircon U–Pb dating of silicic ignimbrites, post-volcanic Xuanwei Formation and clay tuff at the Chaotian section. *Earth Planet. Sci. Lett.* 255, 306–323. doi:10.1016/j.epsl.2006.12.021

Hints, R., Kirsimäe, K., Somelar, P., Kallaste, T., and Kiipli, T. (2006). Chloritization of late ordovician k-bentonites from the northern baltic palaeobasin–influence from source material or diagenetic environment? *Sediment. Geol.* 191, 55–66. doi:10.1016/j.sedgeo.2006.01.004

Hu, Z., Liu, Y., Gao, S., Liu, W., Zhang, W., Tong, X., et al. (2012). Improved *in situ* Hf isotope ratio analysis of zircon using newly designed x skimmer cone and jet sample cone in combination with the addition of nitrogen by laser ablation multiple collector ICP-MS. *J. Anal. At. Spectrom.* 27, 1391–1399. doi:10.1039/c2ja30078h

Hu, Z., Zhang, W., Liu, Y., Gao, S., Li, M., Zong, K., et al. (2015). Wave" signal-smoothing and mercury-removing device for laser ablation quadrupole and multiple collector ICP MS analysis: application to lead isotope analysis. *Anal. Chem.* 87, 1152–1157. doi:10.1021/ac503749k

Koschek, G. (1993). Origin and significance of the SEM cathodoluminescence from zircon. *J. Microsc.* 171, 223–232. doi:10.1111/j.1365-2818.1993.tb03379.x

Liu, Y., Gao, S., Hu, Z., Gao, C., Zong, K., and Wang, D. (2010). Continental and oceanic crust recycling-induced melt-peridotite interactions in the trans-north China orogen: U-Pb dating, Hf isotopes and trace elements in zircons from mantle xenoliths. *J. Petrol.* 51, 537–571. doi:10.1093/petrology/egp082

Liu, Y., Hu, Z., Gao, S., Günther, D., Xu, J., Gao, C. G., et al. (2008). *In situ* analysis of major and trace elements of anhydrous minerals by LA-ICP-MS without applying an internal standard. *Chem. Geol.* 257, 34–43. doi:10.1016/j.chemgeo.2008.08.004

Lu, Z. (1993). Landslides and geotechnical properties of volcanic tuff on Mount Cayley, British Columbia. Thesis. Canada: University of Alberta (Canada) ProQuest Dissertations Publishing.

Ludwig, K. R. (2003). *Isoplot 3.00: a geochronological toolkit for microsoft excel*. California, Berkeley: Berkeley Geochronology Center, 39.

Maeda, H., Kohno, M., Shigenori, H., Sawano, H., and Higaki, S. (2014). Geological characteristics of dip slope type landslides occurred on hard shale dominant formation in the green tuff region: an example of the Oshinkoshin landslide area in the Shiretoko peninsula, east Hokkaido, Japan. *J. Jpn. Landslide Soc.* 51, 1–9. doi:10.3313/JLS.51.81

Masahiro, C. (2016). Disasters caused by deep-seated catastrophic landslides and prediction of their potential sites. *J. Southwest Jiaot. Univ.* 51, 981–986. doi:10.3969/j.issn.0258-2724.2016.05.022

Mo, X., Dong, G., Zhao, Z., Zhu, D., Zhou, S., and Niu, Y. (2009). Mantle input to the crust in southern gangdese, tibet, during the cenozoic: zircon Hf isotopic evidence. *J. Earth Sci.* 20, 241–249. doi:10.1007/s12583-009-0023-2

Olsen, P. E. (1999). Giant lava flows, mass extinctions, and mantle plumes. *Science* 284, 604–605. doi:10.1126/science.284.5414.604

Rampino, M. R., and Stothers, R. B. (1988). Flood basalt volcanism during the past 250 million years. *Science* 241, 663–668. doi:10.1126/science.241.4866.663

Shuzui, H. (2001). Process of slip-surface development and formation of slip-surface clay in landslides in tertiary volcanic rocks, Japan. *Eng. Geol.* 61, 199–220. doi:10.1016/S0013-7952(01)00025-4

Shuzui, H., and Shimoda, S. (1987). Clay minerals of landslide clays in the Kunimi area, Toyama prefecture. *Nendo Kagaku* 27, 211–220. doi:10.11362/jcssjnendokagaku1961.27.211

Trandafir, A. C., and Amini, Z. A. (2009). Yielding mechanism of shallow mass movements in completely decomposed Norwood tuff: the zigzag sign landslide, Utah. *Environ. Geol.* 57, 1443–1451. doi:10.1007/s00254-008-1422-x

Vervoort, J. D., Patchett, P. J., Gehrels, G. E., and Nutman, A. P. (1996). Constraints on early earth differentiation from hafnium and neodymium isotopes. *Nature* 379, 624–627. doi:10.1038/379624a0

Wignall, P. B. (2001). Large igneous provinces and mass extinctions. *Earth-Sci. Rev.* 53, 1–33. doi:10.1016/S0012-8252(00)00037-4

Wu, F., Yang, Y., Xie, L., Yang, J., and Xu, P. (2006). Hf isotopic compositions of the standard zircons and baddeleyites used in U-Pb geochronology. *Chem. Geol.* 234, 105–126. doi:10.1016/j.chemgeo.2006.05.003

Xu, Y. G., He, B., Chung, S. L., Menzies, M. A., and Frey, F. A. (2004). Geologic, geochemical, and geophysical consequences of plume involvement in the Emeishan flood-basalt province. *Geology* 32, 917–920. doi:10.1130/G20602.1

Zong, K., Klemd, R., Yuan, Y., He, Z., Cuo, J., Shi, X., et al. (2017). The assembly of Rodinia: the correlation of early Neoproterozoic (ca. 900 ma) high-grade metamorphism and continental arc formation in the southern Beishan orogen, southern central Asian orogenic belt (Caob). *Precambrian Res.* 290, 32–48. doi:10.1016/j.precamres.2016.12.010